Advances in Water Resources 34 (2011) 128–136

Contents lists available at ScienceDirect

Advances in Water Resources

journal homepage: www.elsevier.com/locate/advwatres

Coupling water flow and solute transport into a physically-based surface–subsurface hydrological model

S. Weill [a,*], A. Mazzia [a], M. Putti [a], C. Paniconi [b]

[a] Dipartimento di Metodi e Modelli Matematici per le Scienze Applicate, Università degli Studi di Padova, Padova, Italy
[b] Institut National de la Recherche Scientifique – Centre Eau, Terre et Environnement (INRS-ETE), Université du Québec, Quebec City, Canada

ARTICLE INFO

Article history:
Received 2 July 2010
Received in revised form 30 September 2010
Accepted 1 October 2010
Available online 13 November 2010

Keywords:
Integrated hydrologic modeling
Surface–subsurface interactions
Flow–transport coupling
Old water/new water paradox
Richards equation
Advection–dispersion equation

ABSTRACT

A distributed-parameter physically-based solute transport model using a novel approach to describe surface–subsurface interactions is coupled to an existing flow model. In the integrated model the same surface routing and mass transport equations are used for both hillslope and channel processes, but with different parametrizations for these two cases. For the subsurface an advanced time-splitting procedure is used to solve the advection–dispersion equation for transport and a standard finite element scheme is used to solve Richards equation for flow. The surface–subsurface interactions are resolved using a mass balance-based surface boundary condition switching algorithm that partitions water and solute into actual fluxes across the land surface and changes in water and mass storage. The time stepping strategy allows the different time scales that characterize surface and subsurface water and solute dynamics to be efficiently and accurately captured. The model features and performance are demonstrated in a series of numerical experiments of hillslope drainage and runoff generation.

1. Introduction

Interactions between atmosphere, land surface, and subsurface processes are one of the major controls on the water budget at the catchment and river basin scales (e.g., [1,2]) and are increasingly accounted for in environmental management, ecological, and climate studies. Surface–subsurface interactions are very complex due to the strong interplay between highly heterogeneous topographic, geologic, and geomorphologic features and the spatio-temporal variability of atmospheric forcings. Although these interactions have been investigated over a wide range of hydrological scales through various experimental and numerical studies (e.g., [3,4]), their influence on hydrological dynamics is not yet fully understood, so that important challenges remain for instance in modeling streamflow generation, performing hydrograph separation analyses, or deciphering the paths and travel times of water and solutes.

The so-called "old water" paradox (e.g., [5–8]) remains one of the major challenges in hydrology as it strongly questions our current understanding of streamflow generation processes. Many experimental studies have been performed in humid and tropical catchments to investigate the quick response of streamflow to rainfall inputs and the related issue of hydrograph separation (see Table 1 in [9]). These field experiments have shown that pre-event or "old water" often dominates the hydrograph response (e.g., [10,11]), a finding that is somewhat puzzling given the relatively slow dynamics of subsurface flow. In arid or semi-arid areas, by contrast, Hortonian runoff is the dominant runoff generation process and streamflow is mainly composed of event water (e.g., [12]).

Although measurement techniques have greatly improved, field studies are not sufficient to fully investigate hydrograph separation or transit time distributions. Following the "virtual experiment" concept presented by Weiler and McDonnel [13], studies based on numerical simulation have recently also begun to tackle these issues (e.g., [9,14–17]). Hydrological models that can describe in a physical and distributed manner the strong coupling between flow and transport and surface and subsurface processes are particularly relevant for such investigations.

In the current generation of distributed-parameter process-based hydrological models, a variety of approaches has been used to couple surface and subsurface flow processes (e.g., [18–22]), whereas only a handful of models has addressed both flow and transport interactions between the land surface and the subsurface (e.g., [23,21]). In this paper, the novel coupling scheme used for the flow model CATHY (CATchment HYdrology), described in Camporese et al. [22], is extended to solute transport phenomena.

* Corresponding author. Present address: Laboratoire d'Hydrologie, de Géochimie de Strasbourg, University of Strasbourg, CNRS, UMR 7517, France.
E-mail addresses: sylvain.weill@engees.unistra.fr (S. Weill), mazzia@dmsa.unipd.it (A. Mazzia), putti@dmsa.unipd.it (M. Putti), claudio.paniconi@ete.inrs.ca (C. Paniconi).

0309-1708/$ - see front matter © 2010 Elsevier Ltd. All rights reserved.
doi:10.1016/j.advwatres.2010.10.001

Surface transport is described by a diffusive wave equation analogous to that used in the flow model, and resolved by the same path-based Muskingum–Cunge scheme, whereas the subsurface transport equation is solved by a time-splitting technique combining flux limited finite volumes and a classical finite element scheme [24]. The coupling approach, based on a boundary condition switching algorithm that determines the partitioning of mass and water exchange fluxes between surface and subsurface, is combined with a sequential solution procedure for the four model components (flow and transport for the surface and subsurface).

Overall, this modeling strategy is computationally efficient (compared to a fully coupled approach that resolves all governing equations simultaneously), modular (numerical schemes can be tailored to each model component, for instance), and it allows nested time stepping that can adapt to different characteristic time scales (for surface vs subsurface processes, for example). Following a presentation of the model that focuses in particular on how the interactions between flow and transport and surface and subsurface are resolved, a series of hillslope test cases is presented to illustrate the model's performance and to investigate issues of hydrograph separation for some simple scenarios.

2. Governing equations and numerical resolution

2.1. Flow module

In the CATHY flow model, the Richards equation [25] and the diffusive wave equation [26] are used to describe variably saturated flow in porous media and surface flow propagation, respectively. For the surface routing component, the same equation, but with different parametrizations, is used for both overland (hillslope) and channel (stream) flow. The system of coupled flow equations can be written as [27,28,22]:

$$S_w S_s \frac{\partial \psi}{\partial t} + \phi \frac{\partial S_w}{\partial t} = \vec{\nabla} \cdot [K_s K_r (\vec{\nabla}\psi + \vec{\eta}_z)] + q_{ss}, \quad (1)$$

$$\frac{\partial Q}{\partial t} + c_k \frac{\partial Q}{\partial s} = D_h \frac{\partial^2 Q}{\partial s^2} + c_k q_s, \quad (2)$$

where $S_w = \theta/\theta_s$ is the water saturation [–], θ is the volumetric moisture content [–], θ_s is the saturated moisture content (generally equal to the porosity ϕ) [–], S_s is the aquifer specific storage [L^{-1}], ψ is the pressure head [L], t is time [T], $\vec{\nabla}$ is the gradient operator [L^{-1}], K_s is the saturated hydraulic conductivity [L/T], $K_r(\psi)$ is the relative hydraulic conductivity [–], $\vec{\eta}_z = (0,0,1)'$, z is the vertical coordinate directed upward [L], q_{ss} is a source (positive) or sink (negative) term [L^3/L^3 T], s is the longitudinal coordinate system used to describe the overland/channel network [L], Q is the surface discharge [L^3/T], c_k is the kinematic celerity [L/T], D_h is the hydraulic diffusivity [L^2/T], and q_s is the inflow (positive) or outflow (negative) exchange rate from the subsurface to the surface [L^3/L T]. Note that q_s has the dimension of a water flux per unit length.

The 3D subsurface flow equation (1) is solved using linear Galerkin finite elements, with tetrahedral elements and a weighted finite difference time integration scheme. A Newton-like iterative algorithm is used to linearize Richards equation. The unsaturated soil hydraulic functions, describing both moisture content and relative permeability, as a function of pressure head, are specified using either the van Genuchten and Nielsen [29], Brooks and Corey [30] or Huyakorn et al. [31] models. Both Dirichlet and Neumann boundary conditions can be imposed on the boundary and inside the subsurface domain, with switching procedures as described later. More details on the numerical aspects and other features of the subsurface flow model can be found in Camporese et al. [22] and in Paniconi and Putti [32].

The 1D surface flow equation (2) is solved using a finite difference explicit in time Muskingum–Cunge algorithm [33] on a one-dimensional drainage network defined starting from a digital elevation model (DEM) representation of the topography. Different methods can be used to extract the drainage directions and to differentiate the hillslope and stream cells [34]. For each DEM cell, the Muskingum–Cunge routing scheme is applied to compute the outgoing water flux based on the incoming flux and the source term q_s calculated by the coupling algorithm [22]. The surface flow celerity is dynamically evaluated using a discharge-dependent relationship resulting from a combination of Manning's equation and the Leopold and Maddock hydraulic geometry relationships [35].

2.2. Transport module

Transport processes in the subsurface and at the land surface are described by the classical 3D advection–dispersion equation [36] and the 1D advection–diffusion equation, respectively. This particular surface transport equation is chosen for compatibility with the land surface flow model. The system of coupled transport equations can be written as:

$$\frac{\partial \theta c}{\partial t} = \vec{\nabla} \cdot [-\vec{U} c + D\vec{\nabla} c] + q_{tss}, \quad (3)$$

$$\frac{\partial Q_m}{\partial t} + c_t \frac{\partial Q_m}{\partial s} = D_c \frac{\partial^2 Q_m}{\partial s^2} + c_t q_{ts}, \quad (4)$$

where c is the subsurface solute concentration [M/L^3], $\vec{U}$ is the Darcy velocity vector [L/T], D [36] is the tensor accounting for both mechanical dispersion and molecular diffusion [L^2/T], q_{tss} is a solute mass source (positive) or sink (negative) term [M/L^3 T], Q_m is the solute mass discharge [M/T], c_t is the kinematic solute celerity [L/T], D_c is the surface solute diffusivity [L^2/T], and q_{ts} is the solute mass inflow (positive) or outflow (negative) exchange rate from the subsurface to the surface [M/L T]. Note that q_{ts} has the dimension of a mass flux per unit length.

The subsurface transport equation (3) is solved using the time-splitting technique presented in [37] and extended to 3D in [24] and [38]. In this two-step scheme, the advective part of Eq. (3) is first solved using a flux limited finite volume method with an explicit time discretization, and the resulting concentration field is then used as initial condition for a finite element based implicit in time formulation that solves the dispersive portion of (3). In our implementation, a linear Galerkin approach is used for the dispersive component, instead of the mixed hybrid scheme used in [37,39], and [24]. The solution procedure allows the use of multiple advective sub-time steps per dispersive time step, with the number of substeps controlled by stability constraints [24]. The high resolution finite volume scheme used for the advective step of the transport equation introduces minimal numerical diffusion even in the absence of physical dispersion, a critical feature for solving advection-dominated problems.

Both prescribed concentration (Dirichlet) and prescribed flux (Neumann or Cauchy) boundary conditions can be imposed on the subsurface boundaries to describe a variety of mass inputs. For numerical consistency, the Dirichlet conditions are specified in the advective part of the solution procedure while Neumann conditions are imposed in the dispersive step. Total Cauchy boundary conditions at the land surface are used to resolve the solute exchange terms q_{tss} and q_{ts} in the transport coupling algorithm as described later. A total Cauchy boundary condition, integrated over the cell area A [L^2], is imposed using the following equation [40]:

$$(D\vec{\nabla} c - \vec{U} c) \cdot \vec{n} = \frac{q_{\text{Cauchy}}}{A}, \quad (5)$$

where $\vec{n}$ is the outward normal unit vector and q_{Cauchy} is the prescribed total flux of solute [M/T].

The surface transport equation (4) is solved with the same numerical formulation used for the surface flow equation, i.e., a finite difference explicit in time matched artificial diffusion algorithm. The incoming and outgoing mass discharges are the dependent variables and are computed for each DEM cell. In the current implementation of the model we assume that solute and water propagate with the same dynamics on the surface, thus the kinematic celerity c_t and the diffusivity D_c in Eq. (4) are set equal to the kinematic celerity c_k and the diffusivity D_h for water. This assumption is probably more realistic for applications at the catchment scale than at the field or laboratory scale or when dealing with point sources of contaminant (where the dispersive behavior at the land surface may be important), although further investigation of this issue is needed.

3. Coupling algorithms

Three levels of coupling are dealt with in the model: (i) surface–subsurface flow coupling, (ii) surface–subsurface transport coupling, and (iii) flow–transport coupling. In the sequential solution approach used in CATHY, coupling is intrinsically linked to time stepping, thus the time stepping strategy is described first. In what follows, "potential fluxes" are denoted R [L^3/T] and refer to the atmospheric inputs, i.e., the time series of precipitation ($R > 0$) and potential evaporation ($R < 0$) rates, while "actual fluxes" q_{act} [L^3/T] refer to the boundary fluxes that are computed after the subsurface flow equation has been solved for pressure heads. Actual fluxes are positive for infiltration and negative for exfiltration.

3.1. Time stepping

The time stepping strategy used in the coupled flow and transport solver is an extension of the procedure described in [22]. The explicit in time nature of the Muskingum–Cunge algorithm makes it possible to use a noniterative sequential procedure to solve the four coupled governing equations. The different steps to evaluate the solution at time t^{k+1} from the solution at time t^k are:

1. solve the surface flow equation (2) using q_s^k as source term to compute Q^{k+1} and its equivalent in ponding head h^{k+1},
2. solve the surface transport equation (4) using q_{ts}^k as source term to compute Q_m^{k+1} and its equivalent in surface concentration c_{surf}^{k+1},
3. use h^{k+1} and the atmospheric inputs to define the surface-to-subsurface water source/sink term q_{ss}^{k+1} and the boundary conditions for the subsurface flow solver,
4. solve the subsurface flow equation (1) to compute the pressure heads ψ^{k+1},
5. compute the subsurface-to-surface water source/sink term q_s^{k+1} using ψ^{k+1} and the balance between potential and actual fluxes, as described in the next section,
6. use ψ^{k+1} to compute the velocity field $\vec{U}^{k+1}$,
7. use c_{surf}^{k+1}, h^{k+1}, and the potential and actual water fluxes to define the surface-to-subsurface mass source/sink term q_{tss}^{k+1} and the boundary conditions for the subsurface transport solver,
8. solve the subsurface transport equation (3) to compute the subsurface concentrations c^{k+1},
9. compute the subsurface-to-surface mass source/sink term q_{ts}^{k+1} using the flow and transport variables needed to perform a consistent solute mass balance, as described in Section 3.3.

For the coupled flow and transport model, time stepping is controlled by the subsurface flow equation. As described in [22], the time step grows and shrinks during a simulation to adapt to the degree of nonlinearity and the intensity and variability of the atmospheric forcing inputs. Multiple surface flow and transport time steps can be taken per subsurface flow step, a feature that allows automatic adaptation to the different time scales of the processes involved. In the time-splitting procedure used in the subsurface transport solution, the dispersive time step is synchronized with the subsurface flow time step, while multiple advective time steps are taken per dispersive step to ensure stability of the finite volume approach.

3.2. Surface–subsurface flow coupling

The terms used to couple the surface and subsurface flow equations are the source/sink terms q_{ss} and q_s of Eqs. (1) and (2), which represent the water flux exchanges between the surface and subsurface domains. The surface-to-subsurface flow contribution q_{ss} and its equivalent in terms of ponding head h are determined after the solution of the surface flow equation (steps 1 and 3 in the above time stepping procedure), using a local mass balance calculation. The subsurface-to-surface flow contribution q_s is evaluated after the solution of the subsurface flow equation (steps 4 and 5). Local conversion between ponding heads [L], volumetric flux [L^3/T], and specific flux [L/T] is readily performed by invoking time step size, channel element length, and cell area values, as is any conversion between the node-based (subsurface) and cell-based (surface) representations of the computational domain.

In CATHY, the partitioning between surface and subsurface flow processes is controlled by the subsurface model, since the atmospheric forcing input is treated as a boundary condition for Eq. (1). The land surface boundary condition is handled by a switching algorithm [27,22] that determines for any given surface node whether a Neumann (i.e., prescribed flux) or Dirichlet (i.e., prescribed head) condition is to be imposed. The type of boundary condition is dictated by the saturation (or pressure) state of the node. A Neumann boundary condition is in effect so long as the surface node is not saturated, in the case of rainfall, or is not dry beyond a minimum threshold moisture content, in the case of evaporative forcing. Thus under Neumann conditions surface–subsurface partitioning is considered as an atmosphere–controlled process and the prescribed flux is set equal to the potential flux. If the surface node becomes saturated during rainfall or overly dry during evaporation, the surface boundary condition is switched to Dirichlet and surface–subsurface partitioning becomes soil-limited. Under Dirichlet conditions the infiltration or exfiltration flux (i.e., the actual as opposed to the potential flux) is calculated from the pressure head solution. This check for boundary condition switching at the land surface is performed at every nonlinear iteration of the subsurface solution procedure.

Once the surface nodal pressure heads and fluxes are known, the subsurface-to-surface source/sink term q_s is evaluated from mass balance considerations. The boundary condition-based coupling procedure thus splits potential atmospheric forcing into actual fluxes across the land surface and changes in surface storage (or ponding heads). This procedure ensures the continuity of both pressure and water flux across the land surface without introducing new parameters, in contrast to other approaches where a linear flux exchange term is explicitly added into the equations (e.g., [18,19]).

3.3. Surface–subsurface transport coupling

The terms used to couple the surface and subsurface transport equations, i.e., the solute source/sink terms q_{tss} and q_{ts} of Eqs. (3)

and (4), represent the exchange of solute between the surface and subsurface domains. Note that q_{tss} includes the total flux imposed on Cauchy boundaries. In the coupling algorithm, local conversion between concentration and mass flux is performed analogously to the flow equation using time step size, channel element length, cell- and node-based surface areas, and water volumes calculated by the flow module.

Since solute transport is dependent on the flow conditions, the different states arising from the surface–subsurface flow coupling described earlier need to be taken into consideration, namely whether ponding occurs, whether the potential flux corresponds to rainfall or evaporation, and whether the actual flux corresponds to infiltration or exfiltration. All possible scenarios are then considered in resolving the surface–subsurface transport interactions which, as with flow interactions, are handled by a boundary condition switching scheme. For each scenario, the flow variables already computed and the surface concentrations are used to determine, via a local solute mass balance calculation, the surface boundary condition for the subsurface transport equation (3). At each surface node, a different type of boundary condition is imposed depending on whether infiltration or exfiltration is occurring. Note that surface nodes that represent point sources of solute (for instance from a contaminant spill) are treated as Dirichlet nodes and are exempt from the boundary condition switching check for the duration of the source input.

Infiltration case. For surface nodes where infiltration is taking place, a total Cauchy boundary condition (i.e., a prescribed total solute flux) is imposed. Two different situations need to be considered: (i) the node is unsaturated and (ii) the node is saturated or ponded. In the case of an unsaturated surface node, the total solute flux is the sum of the contributions from rainfall and surface routing, yielding the following Cauchy boundary condition:

$$q_{\text{Cauchy}} = \max(R,0)c_r + (q_{act} - \max(R,0))c_{surf}, \tag{6}$$

where c_r is the solute concentration associated with the atmospheric input R (equal to 0 if $R<0$), c_{surf} is the concentration at the surface node calculated by the surface transport module, and $(q_{act} - \max(R,0))$ represents the volume of water that accumulates at a given cell as calculated by the surface flow module and converted into a flux using the cell dimension and time step size. Note that c_r in Eq. (6) will often be zero; an example of an application with nonzero c_r would be irrigation with treated wastewater (in this case R would be the irrigation rate). At the end of the time step, since all available (atmospheric plus routing) water has infiltrated, the subsurface-to-surface coupling term q_{ts} for the start of the next time step acts as a sink term and is given by:

$$q_{ts} = -\frac{(q_{act} - \max(R,0))c_{surf}}{\Delta s}, \tag{7}$$

where Δs is the length of the channel segment for the given cell and the minus sign reflects the fact that the solute mass calculated by the surface transport module at the previous time step now needs to be removed from the surface.

In the case of a saturated or ponded surface node, a simple mass balance calculation is performed to update c_{surf} to account for dilution by rainfall or accretion by evaporation. The updated concentration c_{upd} is computed as:

$$c_{upd} = \frac{c_{surf}V_{pond} + \max(R,0)c_r\Delta t}{V_{pond} + R\Delta t}, \tag{8}$$

where V_{pond} is the volume of ponded water at the surface and Δt is the time step size. The resulting Cauchy boundary condition is:

$$q_{\text{Cauchy}} = q_{act}c_{upd}. \tag{9}$$

Correspondingly, the subsurface-to-surface coupling term q_{ts} is computed as the difference between the incoming mass flux from the atmosphere and the mass flux that has infiltrated:

$$q_{ts} = \frac{\max(R,0)c_r - q_{act}c_{upd}}{\Delta s}. \tag{10}$$

Exfiltration case. For surface nodes where exfiltration is taking place, no distinction is needed between unsaturated and ponded situations since water is flowing from the subsurface to the surface (or atmosphere) and thus the water and mass fluxes are determined by the subsurface modules. The solute outflow is purely advective, and the coupling is handled through a zero-Neumann boundary condition (i.e., diffusive flux equal to zero):

$$D\vec{\nabla}c = 0. \tag{11}$$

The subsurface-to-surface coupling term for the exfiltration case is computed as the sum of the subsurface contribution c_{sub} and the atmospheric contribution (if there is one):

$$q_{ts} = \frac{q_{act}c_{sub} + \max(R,0)c_r}{\Delta s}. \tag{12}$$

The transport coupling in CATHY does not explicitly account for diffusive or dispersive exchanges between the surface and subsurface, unlike other models (e.g., [18,9]) where an exchange flux proportional to the concentration difference between the surface and subsurface domains is taken into account. This explicit approach requires the introduction of a new parameter to characterize the diffusive interactions between surface and subsurface. Further study is needed to assess the importance of this diffusive exchanges relative to other phenomena that influence solute interactions between the surface and subsurface.

3.4. Flow–transport coupling

The coupling between the flow and transport modules is seamlessly handled in the sequential solution procedure since the surface and subsurface flow modules are solved before their transport counterparts. The subsurface transport equation needs pressure heads (or, equivalently, moisture contents) from the subsurface flow equation to determine the Darcy velocity and mechanical dispersion terms in Eq. (3), while the surface transport equation needs discharge from the surface flow equation to determine the celerity and diffusivity terms in Eq. (4). In this version of the model we assume that solute concentrations do not affect the flow field (so, for instance, concentrations remain low enough to have a negligible impact on water density and viscosity).

4. Model testing

The validation of the proposed model was carried out following the "virtual experiment" concept presented in [13]. Simulations performed on a synthetic idealized hillslope are used to assess the quality of the model response to problems where the dominant runoff generation process is clearly identified. The different scenarios considered are voluntarily simple so that the response of the hillslope – both for flow and transport – is known a priori, at least qualitatively, based on current theory and experiment. We consider three scenarios: (i) free drainage from a fully saturated hillslope, (ii) infiltration excess (Hortonian) runoff from an initially dry hillslope, and (iii) saturation excess runoff from a hillslope initially in hydrostatic equilibrium.

4.1. Description of the numerical experiments

Fig. 1 shows the geometry of the idealized hillslope. The domain is 10 m long, 10 m wide, and 10 m deep at its lowest point

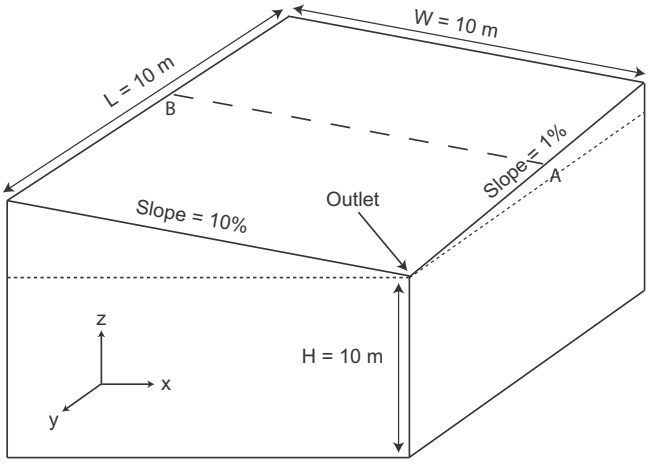

Fig. 1. Geometry of the idealized hillslope.

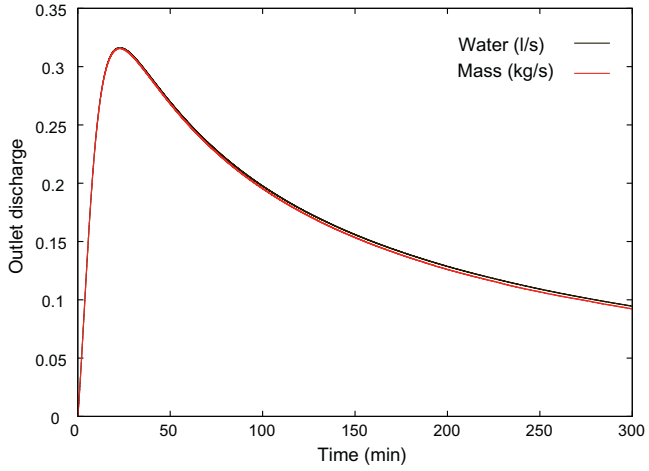

Fig. 2. Water (l/s) and mass (kg/s) discharge at the outlet of the domain.

(i.e., at the outlet). The slopes are 10% and 1% along the x and y directions, respectively. The surface is discretized into 50×50 grid cells (i.e., a DEM resolution of 0.2 m). The subsurface domain is discretized vertically into 32 layers of varying thickness, with each layer parallel to the surface except for the last one, which has a flat base. The layer thicknesses range from 0.05 m at the top to 1 m at the bottom. In three dimensions, each quadrilateral element is subdivided into six tetrahedra, leading to a 3D Delaunay triangulation with 85,822 nodes and 514,998 elements.

The soil parameters were chosen arbitrarily within physically meaningful ranges and are assumed homogeneous and isotropic. The saturated hydraulic conductivity is set to $K_s = 10^{-4}$ m/s, the specific storage to $S_s = 5 \times 10^{-3}$ m^{-1}, the porosity to $\phi = 0.5$, and the van Genuchten fitting parameters for the pressure head–moisture content and pressure head-relative conductivity relationships to $n = 2$ and $\psi_s = -1$ m. No-flow boundary conditions are imposed at the bottom and on the lateral boundaries of the system. For the two runoff scenarios, a constant and spatially homogeneous rainfall is applied at the surface of the domain. All surface parameters were chosen within physically meaningful ranges and are assumed homogeneous in space. All surface cells are considered to be overland (hillslope) with 0.2 m rivulets (i.e., equal to the DEM cell width) and with a Manning–Strickler coefficient equal to 10 m$^{1/3}$ s^{-1}.

For the transport equation, mechanical dispersion is nil (zero dispersivities) and molecular diffusion is negligibly small (diffusion coefficient). With practically zero dispersive mixing, particle tracking can be performed by assigning a unit solute concentration to the "virtual tracer", which is introduced either to the subsurface water (the free drainage scenario) or to the rainfall (the two runoff scenarios).

4.2. Free drainage experiment

This first virtual experiment of drainage from a fully saturated initial condition with no rainfall input is designed to assess the validity of the model when subsurface water (which is tagged at unit initial concentration) is the only contributor to the hydrograph response. The results in terms of water and solute mass discharges at the outlet are presented in Fig. 2. The two hydrographs are virtually identical, as expected, with only small differences observable in the recession limbs. With subsurface water as the only source of exfiltration and outflow, and with no dilution due to mixing, the tracer mass discharge at the outlet is the same as the water discharge. The results also show that the high initial hydraulic gradients (equal to the terrain slope) from a fully saturated domain cause the outlet discharge to quickly reach its peak, followed by a slow recession due to decreasing gradients as exfiltration proceeds.

The small differences between the water and solute hydrographs during the recession are likely linked to the fact that both the Muskingum–Cunge scheme and the velocity fields computed with a classical finite element formulation are not fully conservative [41–46], causing a fraction of the virtual tracer to exit the system through the no-flow boundaries of the domain. These discrepancies are enhanced by the relatively coarse discretization used for the bottom layers of the subsurface domain. To overcome this problem, new reconstruction methods for building conservative velocity fields from standard Galerkin formulations are being studied [47,48]. Note that when rainfall is being tracked (as in the following examples), only a small fraction of the total solute mass in the system reaches the no-flow boundaries, resulting in much smaller mass balance errors.

4.3. Infiltration excess runoff experiment

The second virtual experiment is designed to assess the model for the infiltration excess runoff mechanism. The initial condition is hydrostatic with a horizontal water table located 2 m below the surface with respect to the outlet. A uniform rainfall rate of 2×10^{-4} m/s (i.e., twice the value of the saturated hydraulic conductivity) is applied for a duration of 45 min. The initial condition and rainfall rate and duration were chosen so that the water table never reaches the surface. For this simulation, rainfall water is tagged by setting its concentration equal to one while the concentration of subsurface water is initially set to zero. As with the previous test case, we again obtain, as expected, a mass discharge at the outlet that exactly mirrors the water discharge. In this case the only contribution to the hydrograph response is surface runoff from that portion of rainfall water that exceeds the infiltration capacity of the soil (e.g., [49,50]).

Fig. 3 shows the evolution of the normalized fluxes of total infiltration, outlet discharge, and rainfall falling on saturated areas. The normalization is performed by dividing the fluxes by the rainfall rate. The total infiltration flux and the discharge follow the expected behavior for an infiltration excess process. At early time, all rainfall water infiltrates because of the large head gradient at the soil surface, and no discharge is observed at the outlet. As soon as the soil surface becomes saturated, ponding and surface runoff occur. The time to ponding depends on antecedent soil moisture conditions, which affect the magnitude of the initial hydraulic

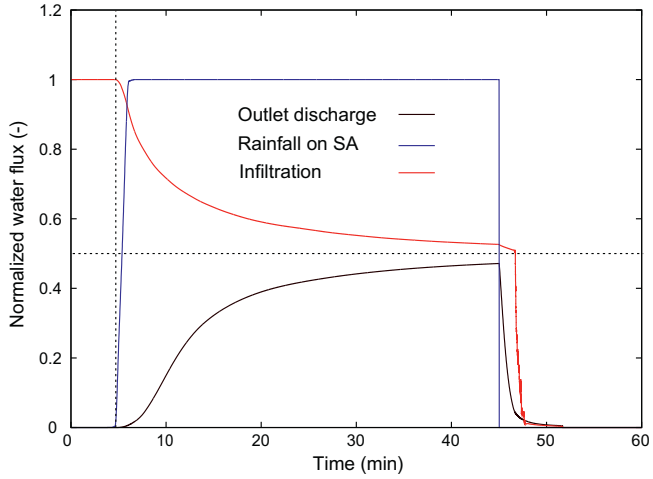

Fig. 3. Evolution of the infiltration flux, the water discharge at the outlet and the rainfall flux falling on saturated areas.

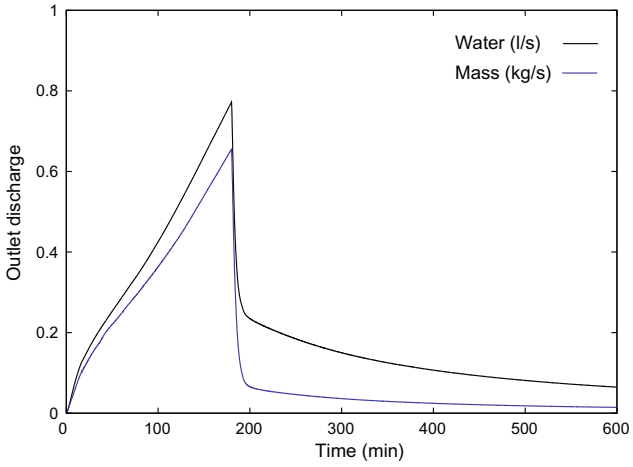

Fig. 4. Water (l/s) and mass (kg/s) discharge at the outlet of the domain.

gradients, and on the ratio between the rainfall rate and the product of the relative and saturated hydraulic conductivities of the soil. We can observe from the behavior of the rainfall flux on saturated areas (Fig. 3) that ponding occurs not quite instantaneously over the entire hillslope, due to a nonuniformity in antecedent unsaturated conditions caused by the initially flat water table relative to a sloping terrain, and to some lateral redistribution of soil water caused by the sloping topography. After ponding time is reached, the infiltration flux decreases smoothly and tends asymptotically to the saturated conductivity (with a normalized value of 0.5). While infiltration decreases, discharge at the outlet increases due to the increasing amount of water that accumulates and runs off at the surface.

4.4. Saturation excess runoff experiment

In this final virtual experiment, the model is assessed for the case where saturation excess runoff is the dominant streamflow generation process. The initial head distribution is hydrostatic with a horizontal water table that intersects the toe of the hillslope (i.e., the outlet). A uniform rainfall rate of 10^{-5} m/s (i.e., 10% of the saturated hydraulic conductivity) is applied for a duration of 3 h. As with the previous test case, rainfall water is tagged by setting its concentration equal to one while the subsurface concentration is initially set to zero.

The surface–subsurface and water–solute dynamics are much more complicated for this test case than for the previous two, for the following reasons: (i) both exfiltration of subsurface water and rainfall falling on saturated areas feed surface runoff; (ii) the capillary fringe ridging mechanism makes the flow and transport response more varied compared to the previous examples [14]; and (iii) the evolution of the saturated areas is highly nonlinear and varies in both time and space. Qualitatively, as soon as some of the rainfall water infiltrates, a saturated area appears close to the outlet. This area expands during the rainfall event, with its dynamics controlled by various geometrical and hydrological parameters such as slope angle, soil characteristics, and antecedent wetness. When rainfall stops, the saturated areas shrink. With this dynamics, water discharging at the outlet will be a mix of event (rainfall) and pre-event (subsurface) water, with the relative contributions of these two sources difficult to predict a priori without a physically detailed and coupled flow and transport model.

Fig. 4 shows the evolution of both water and mass discharge at the outlet of the virtual hillslope. As expected, the rising limb starts very early in the simulation as saturated areas close to the outlet are generated nearly instantaneously. When the rainfall event terminates, discharge drops rapidly as exfiltration remains the only runoff generation mechanism, active on a shrinking saturated area. The flow behavior of the system can also be examined by plotting the evolution of different water fluxes across the land surface (Fig. 5). The results show that during the rainfall period, the infiltration flux decreases as the saturated area and exfiltration flux increase, and that this latter flux remains consistently smaller than the fraction of the surface that is saturated, an observation that is particularly important in interpreting the transport results.

Since precipitation water is tracked with unit input concentration and there is no dispersive mixing, the mass discharge at the outlet reflects solely the event water contribution to the hydrograph. As revealed in Fig. 4, the main contribution to the hillslope outlet response is rainfall falling onto saturated areas. The subsurface water contribution is limited as exfiltration is not the dominant runoff generation mechanism. During the recession phase, the rainfall water contribution is nonzero even though the system dynamics is now controlled entirely by exfiltration. This flux represents water that infiltrated upslope during the rain event and exfiltrates downslope even after the rain has stopped.

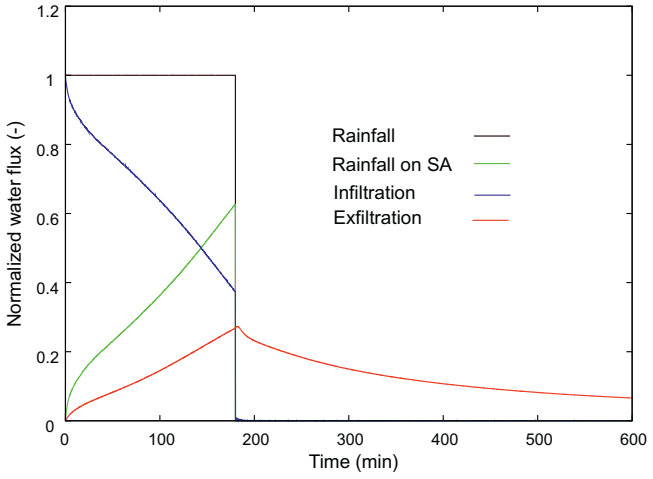

Fig. 5. Normalized rain, infiltration, rainfall on saturated areas (SA), and exfiltration fluxes integrated over the entire hillslope surface. The water fluxes are normalized by the rainfall rate.

To further assess the capabilities of the coupled flow and transport model, the total (hydraulic) head and concentration fields at three different simulation times are presented in Fig. 6. The total head fields after 1 and 2 h show the existence of a groundwater ridge [51], whose influence on pre-event water contributions has recently been investigated [14,16,15]. Three steps for the development of a groundwater ridge can be identified: (i) an initial ridge development; (ii) a transition phase; and (iii) a downslope flow phase. Cloke et al. [14] show how a groundwater ridge can appear at the beginning of the rainfall period due to the influence of the capillary fringe. In this case, the subsurface velocity field drives a portion of the subsurface water to the downslope part of the system, while another portion flows in the opposite direction and contributes to a filling of the upper part of the system. The ridge migrates upslope as time increases and disappears when the upper part of the hillslope becomes more saturated, producing a more regular flow field towards the outlet. In Fig. 6, the three steps described in [14] can be observed, with the hydraulic head fields exhibiting the divergent velocity fields after 1 and 2 h and a more uniform behavior at 3 h.

The concentration fields at the same three times are also presented in Fig. 6, showing the existence in the subsurface domain of a high concentration zone that highlights the areas where rainfall accumulates. During the first two time periods, this accumulation zone is located just downslope of the groundwater ridge, in a region where the hydraulic head gradient is smallest. To better explain this phenomenon, we examine the results at time 1 h along a surface transect that passes through the outlet (Fig. 7), and as a function of time at the outlet (Fig. 8). Fig. 7 shows the existence of three different surface regimes characterized by different ponding and surface flux conditions: at the top of the hillslope, the surface is unsaturated and all rainfall water infiltrates; in the downslope part, the surface is ponded and exfiltration occurs (i.e., negative surface flux); in between these two regions, the surface is ponded and infiltration occurs. These three regimes were observed experimentally by Abdul and Gillham [51]. The results indicate that the higher concentration region is located at the interface between the "full infiltration" and the "ponding and infiltration" zones. The evolution of the total exfiltration flux for both water and mass (Fig. 8) shows that most of the water exfiltrating is subsurface water (i.e., not rainfall water). The small proportion of rainfall water that does contribute to exfiltration does so by infiltrating and thereby bringing the capillary fringe closer to the surface. As a final remark, it is interesting to note that at early times the rainfall water that infiltrates in the "ponding and infiltration" zone gets trapped in the subsurface domain. This phenomenon is linked to the fact that exfiltration of subsurface water close to the outlet prevents rainfall water from exiting the system.

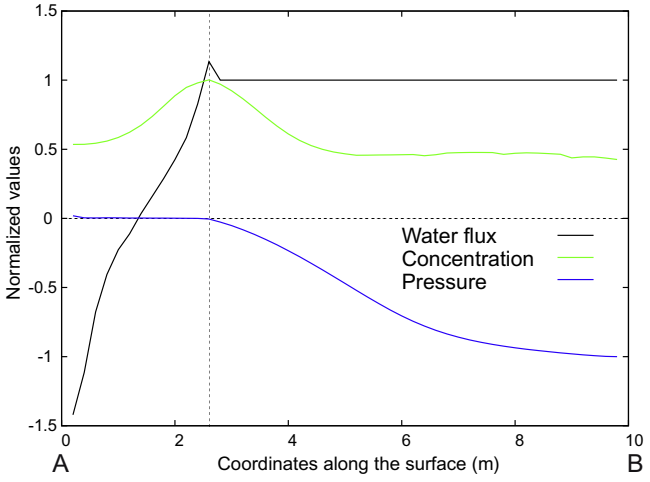

Fig. 7. Normalized surface flux, surface concentration, and surface pressure head along transect AB (see Fig. 1) after 1 h. The surface flux is normalized by the rainfall rate and the surface concentration and surface pressure head by their respective maximum values.

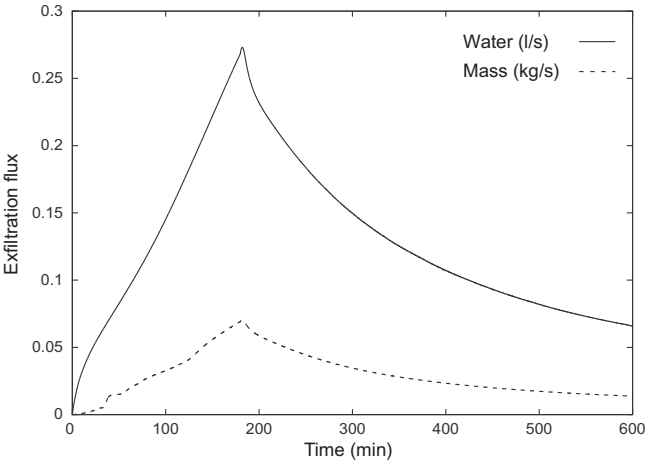

Fig. 8. Evolution of water and mass exfiltration fluxes across the land surface at the hillslope outlet.

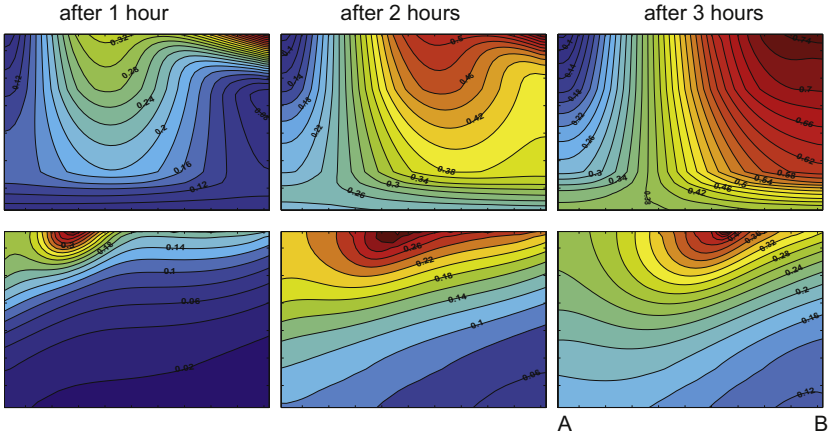

Fig. 6. Vertical cross sections of hydraulic head (top) and concentration (bottom) fields along transect AB (see Fig. 1).

5. Conclusions

A surface–subsurface coupled flow and transport model has been presented. The surface modules use diffusive wave equations to route both water and solute along a surface network composed of both hillslope and channel cells, with different parametrizations for these two elements of the surface domain. The 3D variably saturated subsurface flow equation is solved using classical Galerkin finite elements while the 3D advection–dispersion transport equation is solved with a time-splitting technique that uses finite volumes for the advective part of the equation and Galerkin finite elements for the dispersive part. Surface boundary condition switching algorithms are used to describe the complex flow and transport interactions between the surface and subsurface. These coupling procedures, based on water and solute mass balance considerations, effectively partition atmospheric sources and sinks into water and solute fluxes across the land surface and changes in mass storage on the land surface. The coupling algorithms are designed to provide a physically relevant description of surface–subsurface interactions and to ensure continuity of pressure head and mass concentration. The overall modeling approach allows sequential resolution of the governing equations and the use of nested time stepping that can account for the different dynamics and numerics of surface and subsurface flow and transport phenomena.

Hydrological models that incorporate a detailed description and resolution of surface–subsurface interactions are still evolving, and various approaches are being proposed to deal with coupling, time stepping, and other numerical aspects (e.g., [52,53]). It will be important to assess the relative merits of different approaches, such as the sequential noniterative procedure used in CATHY and the fully implicit procedures used in models such as those presented by [20,23,21]. Model intercomparison studies (e.g., [54]) are an effective means of testing model validity and performance. Benchmark test cases and datasets based on real applications need to be developed and made available in order to further this aim.

The test case used in this paper consists of a virtual idealized hillslope subjected to various drainage and runoff generation simulation experiments. The simulations also demonstrated that coupled surface–subsurface flow–transport models are useful tools for investigating hydrograph separation and related issues such as the "old water" paradox that are much debated in the current literature (e.g., [9,55,56,8]).

Acknowledgments

The financial support of the Ouranos Consortium and the Natural Sciences and Engineering Research Council of Canada (Grant CRDPJ-319968-04), the CARIPARO Foundation (project "Transport phenomena in hydrological catchments: Hydrological and geophysical experiments and modeling"), and the European Commission (Grant FP7-ENV-2009-1-244151) is acknowledged.

References

[1] Winter TC, Harvey JW, Franke OL, Alley WM. Ground water and surface water: a single resource. Circular 1139, US Geological Survey, Denver, CO; 1998.
[2] Sophocleous MA. Interactions between groundwater and surface water: the state of the science. Hydrogeol J 2002;10:52–67.
[3] Harvey JW, Bencala KE. The effect of streambed topography on surface–subsurface water exchange in mountain catchments. Water Resour Res 1993;29(1):89–98.
[4] Storey RG, Howard KWF, Williams DD. Factors controlling riffle-scale hyporheic exchange flows and their seasonal changes in a gaining stream: a three-dimensional groundwater flow model. Water Resour Res 2003;39(2). doi:10.1029/2002WR001367.
[5] McDonnell JJ. A rationale for old water discharge through macropore in a steep, humid catchment. Water Resour Res 1990;26(11):2821–970.
[6] Pearce AJ. Streamflow generation processes: An austral view. Water Resour Res 1990;26(12):3037–47.
[7] Kirchner JW. A double paradox in catchment hydrology and geochemistry. Hydrol Process 2003;17(4):871–4.
[8] McDonnell JJ, McGuire K, Aggarwal P, Beven KJ, Biondi D, Destouni G, et al. How old is streamwater? Open questions in catchment transit time conceptualization, modelling and analysis. Hydrol Process 2010;24:1745–54.
[9] Jones JP, Sudicky EA, Brookfield AE, Park YJ. An assessment of the tracer-based approach to quantifying groundwater contributions to streamflow. Water Resour Res 2006;42:W02407. doi:10.1029/2005WR004130.
[10] Buttle JM. Isotope hydrograph separations and rapid delivery of pre-event water from drainage basins. Prog Phys Geogr 1998;18(1):16–41.
[11] Burns DA. Stormflow-hydrograph separation based on isotopes: the thrill is gone – what's next? Hydrol Process 2002;16(7):1515–7.
[12] Ribolzi O, Karambiri H, Bariac T, Benedetti M, Caquineaux S, Descloitres M, et al. Mechanisms affecting stormflow generation and solute behaviour in a Sahelian headwater catchment. J Hydrol 2007;337(1–2):104–16.
[13] Weiler M, McDonnell JJ. Virtual experiments: a new approach for improving process conceptualisation in hillslope hydrology. J Hydrol 2004;285(1–4):3–18.
[14] Cloke HL, Anderson MG, McDonnell JJ, Renaud JP. Using numerical modelling to evaluate the capillary fringe groundwater ridging hypothesis of streamflow generation. J Hydrol 2006;316(1–4):141–62.
[15] Fiori A, Romanelli M, Cavalli DJ, Russo D. Numerical experiments of streamflow generation in steep catchments. J Hydrol 2007;339(3–4):183–92.
[16] Fiori A, Russo D. Numerical analyses of subsurface flow in a steep hillslope under rainfall: the role of the spatial heterogeneity of the formation hydraulic properties. Water Resour Res 2007;43(7):W07445. doi:10.1029/2006WR005365.
[17] Fiori A, Russo D. Travel time distribution in a hillslope: insight from numerical simulations. Water Resour Res 2008;44(12):W12426. doi:10.1029/2008WR007135.
[18] Vanderkwaak JE, Loague K. Hydrologic-response simulations for the R-5 catchment with a comprehensive physics-based model. Water Resour Res 2001;37(4):999–1013.
[19] Panday S, Huyakorn PS. A fully coupled physically-based spatially-distributed model for evaluating surface/subsurface flow. Adv Water Resour 2004;27:361–82.
[20] Kollet SJ, Maxwell RM. Integrated surface–groundwater flow modeling: a free-surface overland flow boundary condition in a parallel groundwater flow model. Adv Water Resour 2006;29(7):945–58.
[21] Weill S, Mouche E, Patin J. Darcy multi-domain approach for modelling surface/subsurface flow and transport at the plot scale. J Hydrol 2009;366(1–4):9–20.
[22] Camporese M, Paniconi C, Putti M, Orlandini S. Surface-subsurface flow modeling with path-based runoff routing, boundary condition-based coupling, and assimilation of multisource observation data. Water Resour Res 2010;46:W02512. doi:10.1029/2008WR007536.
[23] Therrien R, McLaren RG, Sudicky EA, Panday SM. HydroGeoSphere: a three-dimensional numerical model describing fully-integrated subsurface and surface flow and solute transport. Technical report, Groundwater Simulations Group, Waterloo, Ont., Canada; 2005.
[24] Mazzia AM, Putti M. High order Godunov mixed methods on tetrahedral meshes for density driven flow simulations in porous media. J Comput Phys 2005;208(1):154–74.
[25] Paniconi C, Wood EF. A detailed model for simulation of catchment scale subsurface hydrologic processes. Water Resour Res 1993;29(6):1601–20.
[26] Orlandini S, Rosso R. Diffusion wave modeling of distributed catchment dynamics. J Hydrol Eng ASCE 1996;1(3):103–13.
[27] Bixio AC, Orlandini S, Paniconi C, Putti M. Physically-based distributed model for coupled surface runoff and subsurface flow simulation at the catchment scale. In: Proceedings XIII international conference on computational methods in water resources. Rotterdam, The Netherlands: Balkema; 2000. p. 1115–22.
[28] Putti M, Paniconi C. Time step and stability control for a coupled model of surface and subsurface flow. Proceedings XV international conference on computational methods in water resources, vol. 2. New York: Elsevier; 2004. p. 1391–402.
[29] van Genuchten MT, Nielsen DR. On describing and predicting the hydraulic properties of unsaturated soils. Ann Geophys 1985;3(5):615–28.
[30] Brooks RH, Corey AT. Hydraulic properties of porous media. Hydrology paper 3, Colorado State University, Fort Collins, CO; 1964.
[31] Huyakorn PS, Thomas SD, Thompson BM. Techniques for making finite elements competitive in modeling flow in variably saturated porous media. Water Resour Res 1984;20(8):1099–115.
[32] Paniconi C, Putti M. A comparison of Picard and Newton iteration in the numerical solution of multidimensional variably saturated flow problems. Water Resour Res 1994;30(12):3357–74.
[33] Ponce VM. Diffusion wave modeling of catchment dynamics. J Hydrol Eng ASCE 1986;112(8):716–27.
[34] Orlandini S, Rosso R. Parameterization of stream channel geometry in the distributed modeling of catchment dynamics. Water Resour Res 1998;34(8):1971–85.
[35] Leopold LB, Maddock Jr T. The hydraulic geometry of stream channels and some physiographic implications. Professional paper 252, US Geological Survey, Washington, DC; 1953.

[36] Bear J. Hydraulics of groundwater. New York: McGraw-Hill; 1979.
[37] Mazzia AM, Bergamaschi L, Putti M. A time-splitting technique for advection–dispersion equation in groundwater. J Comput Phys 2000;157(1):181–98.
[38] Mazzia AM, Putti M. Three-dimensional mixed finite element-finite volume approach for the solution of density-dependent flow in porous media. J Comput Appl Math 2006;185(2):347–59.
[39] Mazzia AM, Bergamaschi L, Putti M. On the reliability of numerical solutions of brine transport in groundwater: analysis of infiltration from a salt lake. Transport Porous Med 2001;43(1):65–86.
[40] Bergamaschi L, Mazzia A, Putti M. A time-splitting technique for the solution of density dependent flow and transport in groundwater. In: Computational methods in water resources. Computational methods for subsurface flow and transport, vol. 1. Rotterdam, The Netherlands: Balkema; 2000. p. 75–82.
[41] Forsyth PA. A control volume finite element approach to NAPL groundwater contamination. SIAM J Sci Stat Comput 1991;12(5):1029–57.
[42] Letniowski FW. Three-dimensional Delaunay triangulations for finite element approximations to a second-order diffusion operator. SIAM J Sci Stat Comput 1992;13(3):765–70.
[43] Putti M, Cordes C. Finite element approximation of the diffusion operator on tetrahedra. SIAM J Sci Comput 1998;19(4):1154–68.
[44] Cordes C, Putti M. Accuracy of Galerkin finite elements for the groundwater flow equation in two and three dimensional triangulations. Int J Numer Methods Eng 2001;52:371–87.
[45] Klausen R, Russel T. Relationships among some locally conservative discretization methods which handle discontinuous coefficients. Comput Geosci 2005;8:341–77. doi:10.1007/s10596-005-1815-9.
[46] Putti M, Sartoretto F. Linear Galerkin vs. mixed finite element 2D flow fields. Int J Numer Methods Fluids 2009;60:1011–31.
[47] Larson MG, Niklasson AJ. A conservative flux for the continuous Galerkin method based on discontinuous enrichment. Calcolo 2004;41:65–76. doi:10.1007/s10092-004-0084-7.
[48] Kees CE, Farthing MW, Dawson CN. Locally conservative, stabilized finite element methods for variably saturated flow. Comput Methods Appl Mech Eng 2008;197(51–52):4610–25.
[49] Horton RE. The role of infiltration in the hydrologic cycle. EOS Trans Am Geophys Union 1933;14:446–60.
[50] Rubin J. Numerical analysis of ponded rainfall infiltration. In: Proceedings of the Wageningen symposium. IASH; 1969. p. 440–51.
[51] Abdul AS, Gillham RW. Laboratory studies of the effects of the capillary fringe on streamflow generation. J Hydrol 1984;112(1–2):1–18.
[52] Furman A. Modeling coupled surface–subsurface flow processes: a review. Vadose Zone J 2008;7(2):741–56.
[53] Ebel BA, Mirus BB, Heppner CS, Vanderkwaak JE, Loague K. First-order exchange coefficient coupling for simulating surface water–groundwater interactions: parameter sensitivity and consistency with a physics-based approach. Hydrol Process 2009;23(13):1949–59.
[54] Sulis M, Meyerhoff S, Paniconi C, Maxwell RM, Putti M, Kollet SJ. A comparison of two physics-based numerical models for simulating surface water–groundwater interactions. Adv Water Resour 2010;33(4):456–67. doi:10.1016/j.advwatres.2010.01.010.
[55] Renaud JP, Cloke HL, Weiler M. Comment on an assessment of the tracer-based approach to quantifying groundwater contributions to streamflow. Water Resour Res 2007;43(9). doi:10.1029/2006WR005157.
[56] Sudicky EA, Jones JP, Brookfield AE, Park YJ. Reply to comment by J.-P. Renaud et al. on an assessment of the tracer-based approach to quantifying groundwater contributions to streamflow. Water Resour Res 2007;43(9). doi:10.1029/2006WR005416.